Numerical Study of the Penetration Mechanism and Kinematic Behavior of Drag Anchors Using a Coupled Eulerian-Lagrangian Approach

Haixiao Liu and Yanbing Zhao
School of Civil Engineering, Tianjin University, Tianjin 300072, China
E-mail: liuhx@tju.edu.cn

ABSTRACT: The fundamental properties of drag anchors such as the movement direction of the fluke, the drag angle and drag force at the shackle and the anchor trajectory in soils are closely relevant to the penetration mechanism and kinematic behavior of the drag anchor during installation. In the present work, a large deformation finite element analysis using a coupled Eulerian-Lagrangian approach is performed to simulate the installation process of drag anchors with different fluke sections. The method for determining the reasonable mesh density and drag velocity is proposed based on the investigation on dependency of the numerical results on the mesh density and drag velocity. Through a systematic comparative study between numerical and theoretical analysis, clear knowledge of the movement direction, the drag angle and drag force at the shackle, the anchor trajectory, the effect of anchor geometry and the ultimate embedment depth of the anchor is obtained, which is beneficial to fully understanding the complex behavior of drag anchors in soils.

KEYWORDS: Drag anchor; Penetration mechanism; Kinematic behavior; Movement direction; Drag angle; Drag force; Trajectory; Coupled Eulerian-Lagrangian; Numerical

1. INTRODUCTION

Because of better performance both in pullout capacity and deepwater installation, drag anchors are widely utilized in mooring systems for offshore applications, such as the conventional drag anchor in the catenary mooring system and the vertically loaded plate anchor (VLA) in the taut-wire mooring system. With an anchor handling vessel (AHV) moving along a certain direction, the anchor which initially lies on the seabed, will be gradually penetrated into the soil due to the drag force transmitted from the installation line, as illustrated in Figure 1 (Liu et al. 2010b). Positioning in seabed soils is significant for drag anchors because the pullout capacity of the anchor relies on the embedment depth and orientation of the anchor and the properties of surrounding soils. Therefore, it is important to accurately predict the anchor trajectory in a practical engineering based on a full knowledge of the penetration mechanism and kinematic behavior of drag anchors.

Commercially available drag anchors are always characterized by their complex geometries, which are usually simplified by researchers in the analysis as an anchor with a plate fluke moving along its fluke surface (Stewart 1992; Neubecker and Randolph 1996; Thorne 1998; Elkhatib and Randolph 2005; Aubeny and Chi 2010). However, the anchor geometry generally has much effect on the movement direction of the anchor, which directly influences the anchor trajectory. O'Neill et al. (1997) and O'Neill and Randolph (2001) demonstrated by centrifuge tests that, for a small-scale Vryhof Stevpris anchor, the fluke moves along a plane lying between its top and bottom surfaces. Numerical research by O'Neill et al. (2003) showed that the fluke angle is 24° when the rectangular anchor reaches its ultimate embedment depth (UED), and the wedge anchor travels along a plane lying 4.5° below its bottom surface at the UED. Both experimental and theoretical analysis were performed by Liu et al. (2012b), which proved that the movement direction of the anchor with a rectangular section is along the surfaces (top surface or bottom surface) of the fluke, and the movement direction of the anchor with a wedged section is along its bottom surface. The anchor trajectory is very sensitive to the movement direction of the anchor. If the movement direction decreases slightly, the estimated UED of the anchor will obviously decrease so that a much different anchor trajectory is induced (Liu et al. 2010a).

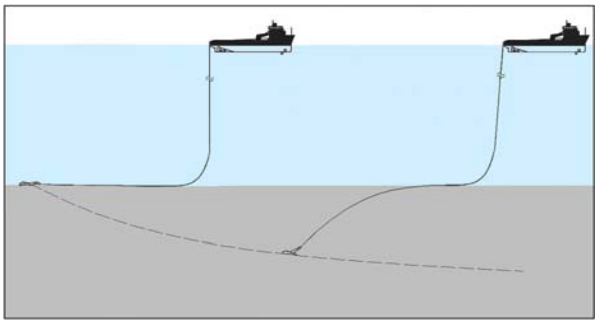

Figure 1 Sketch of the drag anchor installation (Liu et al. 2010b)

During penetration of a drag anchor in seabed soils, complex interaction happens between the anchor and the installation line. However, the interaction can be equivalently analyzed by investigating the drag angle and drag force at the shackle (Zhang et al. 2014). The anchor trajectory is also influenced by the drag angle at the shackle (Liu et al. 2012a), which is closely relevant to the anchor geometry such as the shank angle. Neubecker and Randolph (1996), O'Neill et al. (1997), O'Neill and Randolph (2001) and O'Neill et al. (2003) observed that the drag angle is smaller than the shank angle in their analysis of drag anchors. However, researches by Elkhatib and Randolph (2005) and Aubeny et al. (2008) showed that values of the drag angle are 12° and 3~8° bigger than the shank angle, respectively. Experimental investigation by Liu et al. (2010b) demonstrated that, for drag anchors with flexible shanks, the drag angle is almost a constant during dragging and equals the shank angle. A formula was recently derived by Zhang et al. (2014) for predicting the drag angle at the shackle, which is expressed in terms of key geometries of the anchor.

Obviously, the fundamental properties of drag anchors such as the movement direction of the fluke, the drag angle and drag force at the shackle and the anchor trajectory in soils are closely relevant to the penetration mechanism and kinematic behavior of the anchor during installation. To fully understand the complex behavior of drag anchors in soils, a clear knowledge of these fundamental properties is required by performing a systematic investigation on them. In the present work, a large deformation finite element (FE) analysis using a coupled Eulerian-Lagrangian (CEL) approach is carried out to simulate the installation process of drag anchors with different fluke sections. The dependency of the numerical results on the mesh density and drag velocity is investigated at first to determine the reasonable mesh density and drag velocity. A systematic comparative study between numerical and theoretical analysis is then performed to investigate the movement direction, the drag angle and drag force at the shackle, the anchor trajectory, the effect of anchor geometry and the ultimate embedment depth of the anchor.

2. NUMERICAL MODEL

A three dimensional FE analysis using a CEL approach is performed to simulate the installation process of drag anchors and to analyze the penetration mechanism and kinematic behavior of the anchor in clayey soils. The installation of drag anchors that involves large deformation of surrounding soils can not be solved by the classical FE method, since the large mesh distortion and contact problem will occur so that a convergent problem appears. To overcome these problems, the CEL approach implemented in the commercial software Abaqus (Dassault Systems 2010) is adopted in the present work. For a general geotechnical problem, the structure is modeled as the Lagrangian material, while the soil as the Eulerian material. The contact between Eulerian and Lagrangian materials is enforced by a general contact that is based on a penalty contact method. More details of the CEL technique can be found in the reference (Dassault Systems 2010).

2.1 Simulation of the installation line and drag anchor

During installation of a drag anchor, the installation line transmits the drag force to make the anchor penetrate into the soil, which is difficult to be simulated in the FE analysis. Zhao and Liu (2013) constructed the installation line by connecting cylindrical units with each other using LINK connector elements, as shown in Figure 2(a), in which each unit was modeled as a 3D rigid solid. The LINK provided a pinned rigid link between two nodes to keep the distance between the nodes constant. By simulating the installation line gradually cutting through the soil as it is tensioned by enforcing a constant velocity at the drag point, and comparing with theoretical solutions to the tension at the attachment point and the profile of the embedded line, the efficiency of the FE simulation of line-soil interactional problems was well verified. In the present work, the method for constructing the installation line by Zhao and Liu (2013) is still adopted for simulating the drag anchor installation.

Four anchor models, including one rectangular anchor and three wedge anchors, are designed in the FE analysis, as illustrated in Figure 2(b). The three wedge anchors only differ in the fluke section. The first wedge anchor, of which the top surface is longer than the bottom surface, is labelled Wedge 1. The second wedge anchor, which has an isosceles-triangle section, is labelled Wedge 2. The third wedge anchor, of which the bottom surface is longer than top surface, is labelled Wedge 3. Main parameters of the anchor models are listed in Table 1, in which L_f, B and t are the length, width and thickness of the fluke, respectively, L_s denotes the length (along the central line) of the shank and the central line of the shank passes through the center of mass of the fluke, θ_s is the shank angle, and θ_w is the wedge angle of the wedge anchor, as illustrated in Figure 2(b). The attachment point is located at the top of the shank.

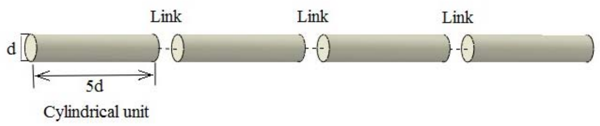

(a)

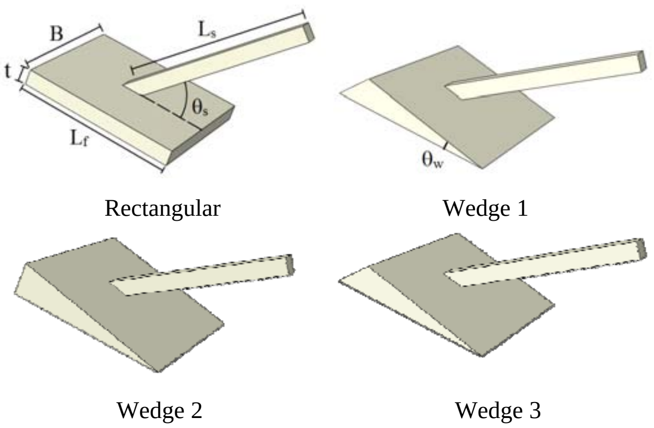

(b)

Figure 2 Modelling the drag anchor and installation line:
(a) the connecting type and dimensions of the installation line;
(b) anchor models

Table 1 Main parameters of anchor models

Anchor	Rectangular	Wedge 1	Wedge 2	Wedge 3
L_f (m)	2	2 1.7	2 2	1.7 2
B (m)	2	2	2	2
t (m)	0.2	-	-	-
L_s (m)	2.4	2.4	2.4	2.4
θ_s (°)	45	45	45	45
θ_w (°)	-	12	12	12

2.2 Property of the soil and contact formulation

The clay is modeled by an elastic-perfectly plastic material with a Mises failure criterion. The soil is assumed to be undrained such that the Poisson's ratio is taken as 0.49, while the Young's modulus $E = 500s_u$ is adopted, where s_u is the undrained shear strength of clay. A linear strength profile $s_u = s_{u0} + kz$ is used in the present work, in which s_{u0} is the shear strength at the seafloor, k is the gradient of shear strength with depth, and z is the soil depth. The soil is discretized by the Eulerian mesh, which needs to extend over the geometry of the soil because there must be a material-free (void) to simulate the deformation of the soil on the seafloor. Due to symmetry of the problem, only half of the installation line, drag anchor and soil domain is analyzed in a 3D space, as illustrated in Figure 3. It should be noted that the soil domain has a T-shape top view to improve the computational efficiency. Parameters of the FE model are listed in Table 2, in which L, $W_{\max}$, $W_{\min}$ and D denote the length, maximum width, minimum width and depth of the soil domain, respectively, L_i is the length of the installation line initially lying on the seafloor, d is the diameter of the installation line, γ'_{soil} is the submerged unit weight of the soil, μ is the frictional coefficient between the structures (including installation line and drag anchor) and the soil, and γ'_{line} and γ'_{anchor} are the submerged unit weights of the installation line and the anchor, respectively.

The contact between the structures and the soil is enforced by a general contact that is based on a penalty contact method. The general contact algorithm, which allows simple definitions of contact with very few restrictions on the types of surfaces involved, is well suited to simulate highly non-linear problems involving large deformations (Dassault Systemes 2010). The Coulomb friction contact is used in the present work. The shear stress τ between the contact surfaces is calculated by $\tau = \mu\sigma$, in which σ is the normal contact pressure. Note that the friction coefficient μ is an input parameter in the FE model but different from the adhesion factor α generally used in geotechnical engineering. Due to that the value of α varies in the range (0, 1) and corresponds to a small value of μ, μ =0.1 is selected in the numerical simulation.

2.3 Effects of the mesh density and drag velocity

Before the systematic study on the installation problem of drag anchors, the dependency of the numerical results on the mesh density and drag velocity is investigated employing the rectangular anchor. The calculated results include the movement direction of the anchor, the drag angle and drag force at the shackle, and the anchor trajectory.

Three meshes with different coarseness are used, as listed in Table 3, in which L_u is the length of the cylindrical unit for constructing the installation line, and B is the width of the anchor fluke. The numerical simulation results at different mesh densities are presented in Figure 4. The movement direction of the anchor θ_m and the drag angle to the top surface of the fluke at the shackle θ_a are almost constant after the drag distance of 1B, as observed in Figures 4 (a) and (b), so the average values of the two parameters, denoted by $\overline{\theta_m}$ and $\overline{\theta_a}$, are also calculated and listed in Table 4 to evaluate the effects of the mesh density and drag velocity. It can be seen that the numerical results converge with decreasing element size. Allow for both the accuracy and efficiency of the simulation, Mesh B is selected in the following analysis. As recommended by Mesh B in Table 3, a reasonable meshing of the soil can be achieved for FE simulation of drag anchor installation by conforming with the meshing criteria established between the key dimensions of the anchor and the anchor line, including the width of the anchor fluke, the diameter of the installation line, and the length of the cylindrical unit for constructing the installation line.

The penetration of a drag anchor in seabed soils is simulated by enforcing a constant drag velocity v at the drag point, as illustrated in Figure 3. Note that this velocity will influence the behaviors of the anchor during installation, such as the penetration depth of the anchor and the soil resistances (Dahlberg and Storm 1999). Four velocities are selected to investigate the effect of drag velocity, including $B/8$ s^{-1} (0.25m/s), $B/4$ s^{-1} (0.5m/s), $B/2$ s^{-1} (1m/s) and B s^{-1} (2m/s). The numerical simulation results are presented in Figure 5, in which only three drag velocities are presented to demonstrate more clearly. Values of $\overline{\theta_m}$ and $\overline{\theta_a}$ at different drag velocities are also listed in Table 4. It is revealed that the movement direction and the drag angle slightly decrease with decreasing value of drag velocity. However, a reduction in drag velocity will result in a significant drop in drag force. The trajectory of the anchor at the large velocity B s^{-1} is very different from those at the small velocities $B/4$ s^{-1} and $B/8$ s^{-1} at the earlier penetration stage,

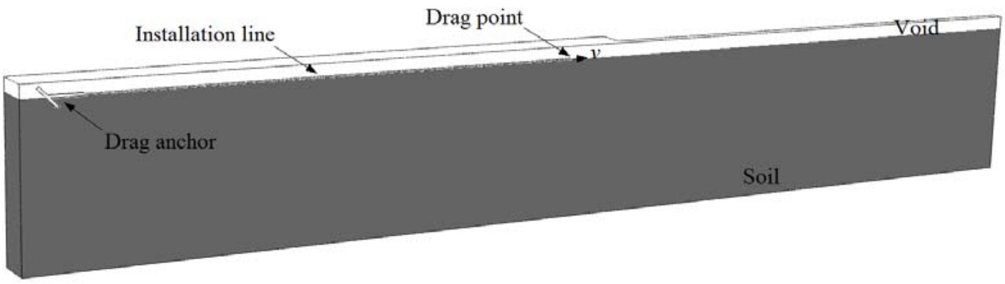

(a)

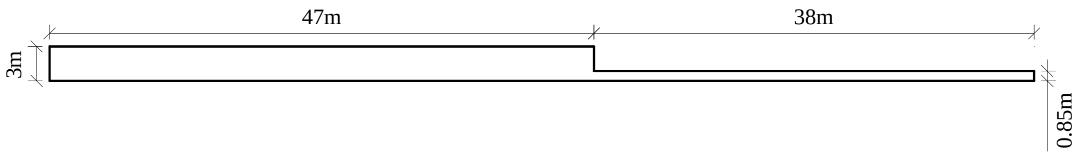

(b)

Figure 3 FE model in simulating the drag anchor installation: (a) FE model; (b) planform of the FE model

Table 2 Parameters in simulating the drag anchor installation

$L \times W_{max} \times D$ (m)	W_{min} (m)	L_i (m)	s_u (kPa)	d (m)	γ'_{soil} (kN/m^3)	μ	γ'_{line} (kN/m^3)	γ'_{anchor} (kN/m^3)
$85\times3\times13$	0.85	37.8	$5+1.5z$	0.1	7	0.1	68	68

Table 3 Mesh density of the soil in the FE model

Case	Mesh size in the direction normal to the movement plane of the anchor				Global size	Element number
	Beneath the anchor line	Beneath the shank	Beneath the fluke	Beyond the anchor		
Mesh A	$d/2$	$d/2$	$d/2 \sim B/10$	$B/10$	$L_u/3$	415124
Mesh B	$d/4$	$d/4$	$d/4 \sim B/10$	$B/10$	$L_u/4$	875420
Mesh C	$d/6$	$d/6$	$d/6 \sim B/10$	$B/10$	$L_u/5$	1648640

while the final penetration depths are nearly the same. If the drag velocity gets larger and larger, the anchor may overturn on the seafloor at the start of dragging and can not penetrate into the soil at all. For the comparative study with the theoretical model based on the limit equilibrium condition, a small drag velocity $B/4\,\mathrm{s}^{-1}$ is recommended in the subsequent analysis. To ensure the installation process being a quasi-static simulation, the ratio of kinetic energy to internal energy should be monitored during the whole installation process and typically less than 10% (Dassault Systems 2010). The maximum ratio of kinematic energy to internal energy of the FE model at the velocity of $B/4\,\mathrm{s}^{-1}$ is only 1.8%.

Table 4 Values of $\overline{\theta_m}$ and $\overline{\theta_a}$ at different mesh densities and drag velocities

Case	Mesh density	Drag velocity (s^{-1})	$\overline{\theta_m}$ (°)	$\overline{\theta_a}$ (°)
1	Mesh A		-6.5	41.5
2	Mesh B	$B/2$	-5.3	40.9
3	Mesh C		-5.1	40.7
4		B	-5.4	41.0
5	Mesh B	$B/4$	-4.7	40.6
6		$B/8$	-4.5	40.5

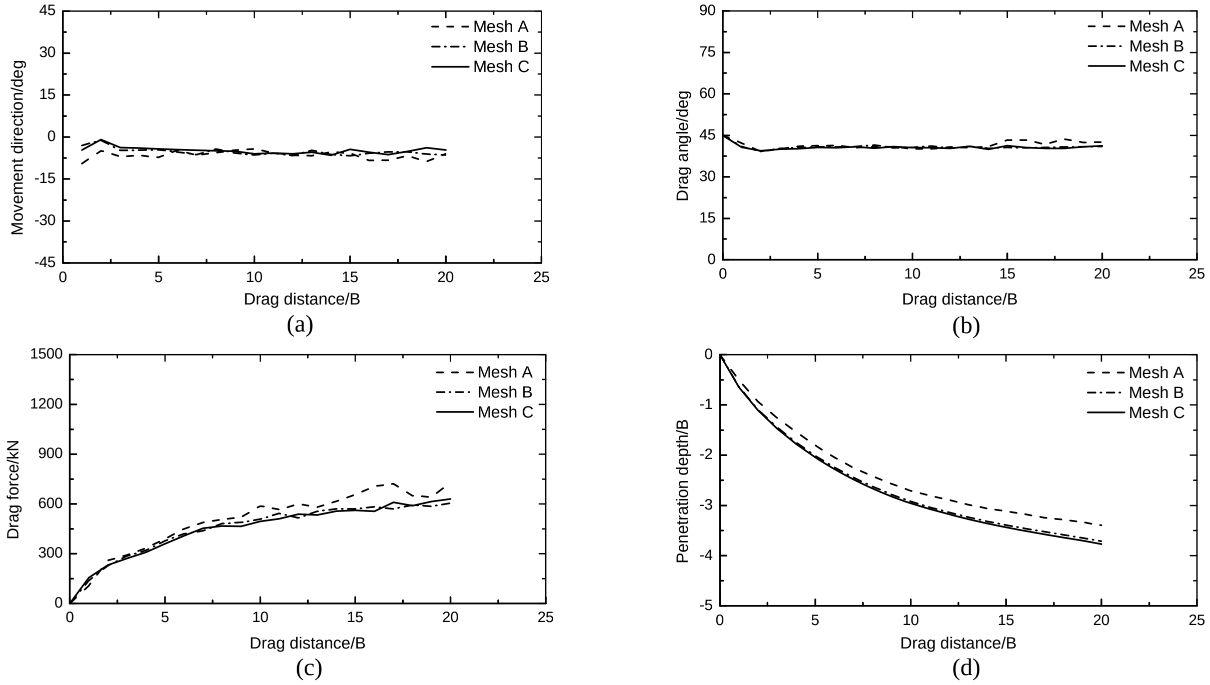

Figure 4 Numerical simulation results at different mesh densities: (a) movement direction; (b) drag angle; (c) drag force; (d) trajectory

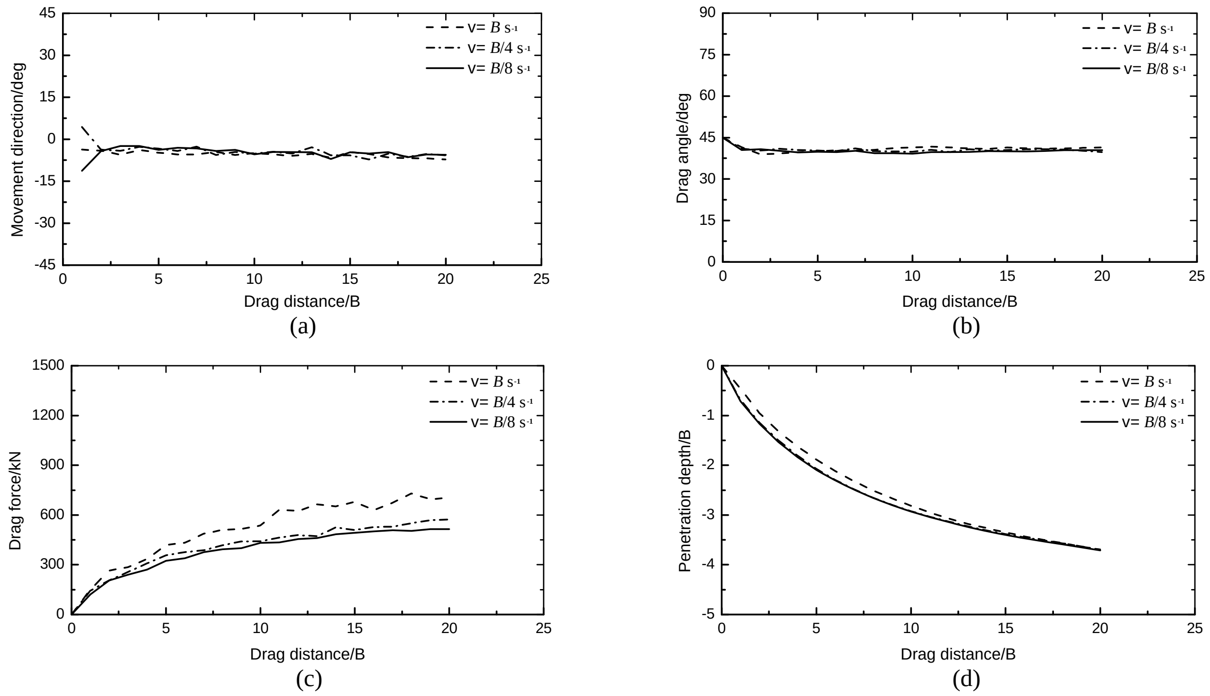

Figure 5 Numerical simulation results at different drag velocities: (a) movement direction; (b) drag angle; (c) drag force; (d) trajectory

3. COMPARATIVE STUDY

A large deformation FE analysis using the CEL approach was carried out by Zhao and Liu (2014) to simulate the installation of drag anchors both in uniform and linear clay. By comparing with theoretical predictions, the efficiency of the FE simulation was well verified. In this section, the penetration mechanism and kinematic behavior of drag anchors are investigated in detail by the FE simulation using the designed four anchor models. Meanwhile, theoretical analysis is also performed based on the work by Liu et al. (2012b, 2013) and Zhang et al. (2014).

Before the comparative study, two important parameters used in the theoretical analysis need to be discussed, i.e., the bearing capacity factors N_{cl} and N_{cf} for the anchor line and the anchor, respectively. For the embedded wire and chain, Vivatrat et al. (1982), Yen and Tofani (1984), and DNV (2000) suggested that the values of N_{cl} be between 9 and 11, 8.4 and 11, and 9 and 14, respectively. However, Degenkamp and Dutta (1989) directly used the Skempton's bearing capacity formula, and suggested the value of N_{cl} as 7.6. Hence, the value of N_{cl} generally varies in the range (7.6, 14), and the mean value 10.8 is adopted in the theoretical analysis.

For a deeply buried anchor, Rowe (1978) and Merifield et al. (2001) suggested that the values of N_{cf} be between 10.28 and 11.42, and 11.16 and 11.86, respectively, while $N_{cf} = 9$ and $N_{cf} = 11.87$ were adopted by Neubecker and Randolph (1996) and O'Neill et al. (2003), respectively. Elkhatib and Randolph (2005) stated that, the value of N_{cf} depends on the ratio of width to thickness of the fluke. If the ratios are 7 and 20, the values of N_{cf} are 9.1 and 11.7, respectively. However, Thorne (1998) and Ruinen (2004) adopted $N_{cf} = 7.6$ directly in their study on drag embedment anchors, which was initially proposed by Skempton. To sum up, the value of N_{cf} generally varies in the range (7.6, 11.87), and hence the mean value 9.7 is adopted in the theoretical analysis.

3.1 Movement direction

The movement direction of the anchor means the penetration orientation of the fluke, which is tangent to the anchor trajectory. Considering that movement directions at different points on the fluke may be not identical, six typical points on the fluke are selected to investigate the movement direction of the anchor model, as illustrated in Figure 6, where Point 6 represents the centre of mass of the fluke. Being an example, the numerical calculated movement direction at Point 6 of Wedge 1 is presented in Figure 7, which shows that the movement direction looks stable and keeps almost a constant after the drag distance of 1B. Values of $\overline{\theta_m}$ at the typical points of the four anchor models are calculated and listed in Table 5, which demonstrates that the value of $\overline{\theta_m}$ at Point 1 is nearly identical with that at Point 5, and the value of $\overline{\theta_m}$ at Point 2 is nearly identical with that at Point 4. These mean that there is almost no difference between the movement directions at the top and bottom surfaces of the fluke. The value of $\overline{\theta_m}$ at Point 1 is a little smaller than that at Point 3 except the Wedge 1 model. Generally, it can be drawn that the movement directions at different points on the fluke are nearly the same and not influenced by the anchor geometry. Hence, the movement direction at Point 6 is reasonable to represent the movement direction of the anchor in soils, which is selected for the following comparative study.

The theoretical solution from Liu et al. (2012b) is also adopted to investigate the movement directions of the four anchor models. Note that only one movement direction of the fluke can be obtained from the theoretical analysis. The parameters necessary for the theoretical prediction can be found in Tables 1 and 2. It should be emphasized that, the adhesion factor α used in the theoretical prediction is calculated utilizing the shear force obtained from the numerical simulation results, i.e., $\alpha = F_s / A_s$, in which F_s is the total shear force on the anchor and A_s is the effective shear area of the anchor. The calculated values of α are 0.42, 0.46, 0.51 and 0.47 for the rectangular anchor, Wedge 1, Wedge 2 and Wedge 3, respectively. The drag angle at the shackle θ_a just equals the shank angle, i.e., 45° for the four anchor models, which is calculated by the method from Zhang et al. (2014).

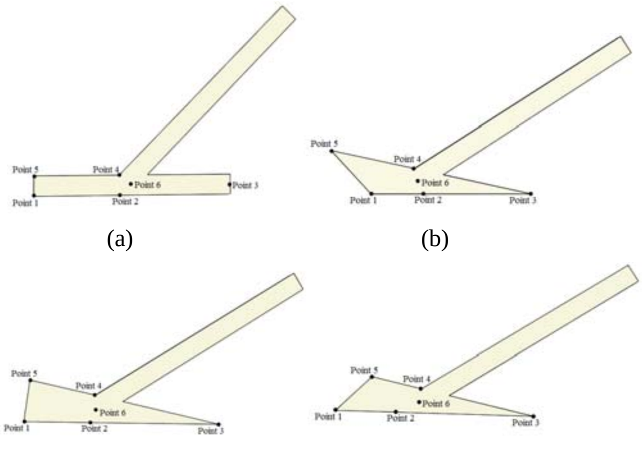

Figure 6 Typical points on the fluke: (a) rectangular anchor; (b) Wedge 1; (c) Wedge 2; (d) Wedge 3

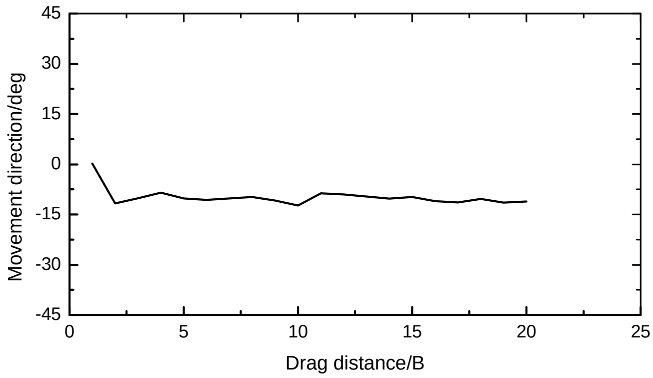

Figure 7 Movement direction at Point 6 on Wedge 1

Table 5 Values of $\overline{\theta_m}$ at typical points on the fluke

Anchor	Point 1	Point 2	Point 3	Point 4	Point 5	Point 6
Rectangular	-4.2°	-4.7°	-5.3°	-4.8°	-4.3°	-4.7°
Wedge 1	-10.4°	-10.3°	-10.2°	-10.4°	-10.4°	-10.4°
Wedge 2	-10.2°	-10.6°	-11.3°	-10.5°	-10.3°	-10.6°
Wedge 3	-11.3°	-11.5°	-11.8°	-11.5°	-11.4°	-11.5°

Movement directions of the four anchor models obtained from numerical and theoretical analysis are presented in Figure 8. It is observed from Figure 8(a) that, for the rectangular anchor, the numerical simulation results are almost constant and the value of

$\overline{\theta_m}$ is -4.7°, i.e., the anchor travels along a plane lying 4.7° below the bottom fluke surface; the predicted values by Liu et al. (2012b) are a constant which equals 0°, i.e., the anchor moves along the surfaces (top surface or bottom surface) of the fluke. The discrepancy between the numerical and theoretical analysis may be caused by the drag velocity and the blunt tip of the rectangular anchor, as analyzed in Sections 2.3 and 3.1, respectively. Figure 8(b) demonstrates that, for the wedge anchors, the numerical results are almost constant and the values of $\overline{\theta_m}$ are -10.4°, -10.6° and -11.5° for Wedge 1, Wedge 2 and Wedge 3, respectively, which means the fluke moves along a plane lying between its top and bottom surfaces but approaching the bottom surface; the predicted movement directions of the three wedge anchors are a constant which equals -12°, which means the anchor moves along its bottom surface. The numerical results also prove that for the wedge anchors, the movement direction of the anchor decreases a little with decreasing ratio of the top length to the bottom length.

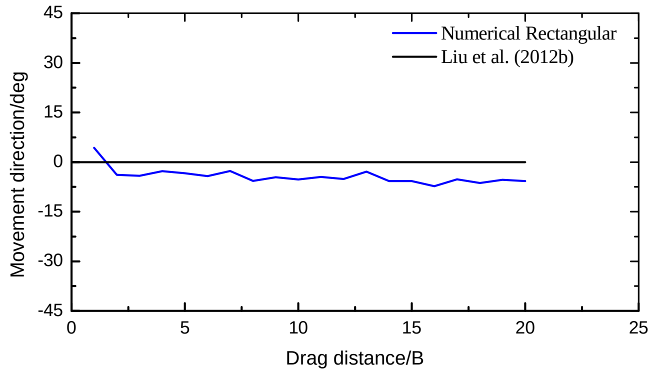

(a)

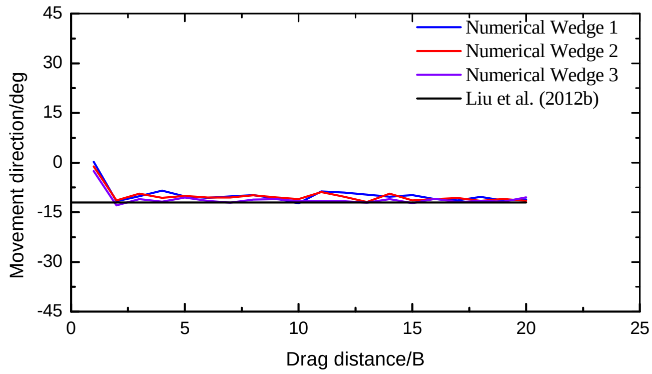

(b)

Figure 8 Movement directions from numerical and theoretical analysis: (a) rectangular anchor; (b) wedge anchors

3.2 Drag angle at the shackle

The drag angle at the shackle θ_a can be simply obtained through the theoretical solution by Zhang et al. (2014), which is expressed in terms of geometric parameters of the anchor as the following:

$$\theta_a = \arctan\left(\frac{y_{shackle} - y_m}{x_{shackle} - x_m}\right) = \arctan\left[\frac{\left(2 + \frac{m_s}{m_f}\right)\sin\theta_s}{\left(2 + \frac{m_s}{m_f}\right)\cos\theta_s - 2\frac{L_1}{L_s}}\right]$$

$$0 < \theta_a < \pi/2 \qquad (1)$$

where, (x_m, y_m) and $(x_{shackle}, y_{shackle})$ denote the position coordinates of the centers of mass of the anchor and the shackle, respectively, m_f and m_s are the masses of the fluke and the shank, respectively, L_1 denotes the distance from the center of mass of the fluke to the shank-fluke attachment point, and L_s denotes the length of the shank. Due to that the central line of the shank passes through the center of mass of the fluke for the four anchor models, the value of L_1/L_s equals zero and hence the value of θ_a calculated by Eq. (1) equals the shank angle of θ_s, i.e., 45°.

Drag angles of the four anchor models obtained from numerical calculation and theoretical prediction are presented in Figure 9. The numerical results are almost constant during installation, and the values of $\overline{\theta_a}$ are 40.6°, 35.4°, 39.2° and 39.4° for the rectangular anchor, Wedge 1, Wedge 2 and Wedge 3, respectively. The numerical values of $\overline{\theta_a}$ are nearly identical and smaller than the fluke-shank angle except Wedge 1. The predicted drag angles are a constant which equals 45° for all anchor models. Note that the four anchor models have an identical shank including the shank angle, and the central line of the shank passes through the center of mass of the fluke. Therefore, it can be drawn from both the numerical and theoretical analysis that the drag angle is closely relevant to the anchor geometry. The drag angle will be determined by the specific shank angle and the connecting type between the shank and the fluke, although the numerical calculated drag angles are smaller than the theoretical predictions. However, the numerical calculated drag angle of Wedge 1 is somewhat smaller than those of other anchor models. The reason is still not clear and needs to be further explored.

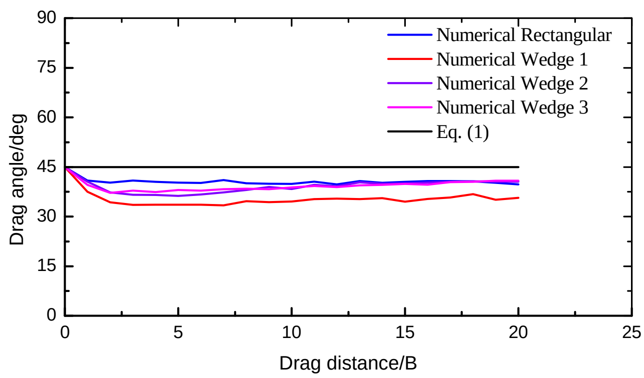

Figure 9 Drag angles at the shackle from numerical and theoretical analysis

3.3 Drag force at the shackle

A theoretical expression of the drag force at the shackle derived by Zhang et al. (2014), in which the anchor line angle at the seafloor is assumed to be zero, can be represented by

$$T_a = \frac{(1+\mu^2)\int_0^{z_a} N_{cl} E_n ds_u dz}{e^{\mu\theta_{ah}} - \cos\theta_{ah} - \mu\sin\theta_{ah}} \qquad (2)$$

where, E_n is the multiplier to give the effective width in the normal direction, z_a is the penetration depth of the shackle, and θ_{ah} denotes the angle subtended by the anchor line to the horizontal at the shackle. It is seen that the unknown parameters in Eq. (2) include N_{cl}, μ, E_n, z_a and θ_{ah}. Values of z_a and θ_{ah} are obtained directly from the numerical simulation results, and the value of μ is the same as that used in the FE model. The anchor

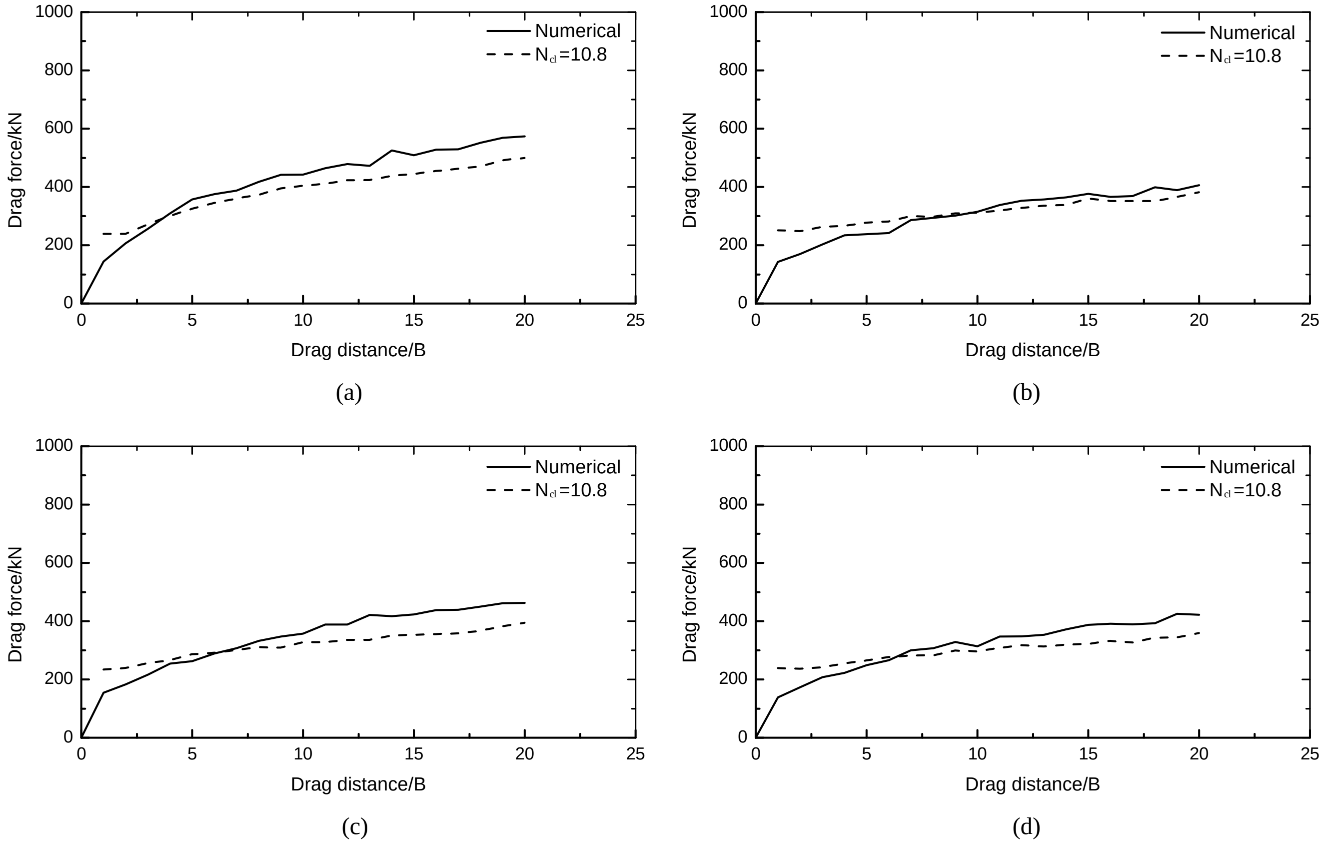

Figure 10 Drag forces at the shackle from numerical and theoretical analysis: (a) rectangular anchor; (b) Wedge 1; (c) Wedge 2; (d) Wedge 3

line simulated in the present work has a circular cross section, so the value of E_n is 1.0 (Degenkamp and Dutta 1989). The value of N_{cl} is selected as 10.8, as discussed earlier.

Drag forces at the shackle of all anchor models obtained from numerical calculation and theoretical prediction are presented in Figure 10, which demonstrates that values of T_a obtained from numerical analysis are generally lager than theoretical predictions, but they are smaller than the calculated values of T_a if the upper bound value 14 is assigned to N_{cl}. It should be noted that, at the start of dragging, the value of θ_{ah} is 0°, so the drag force calculated by Eq. (2) has an infinite value, which does not conform with the physical reality. In Section 2.3, it is demonstrated that the drag force increases with increasing drag velocity, which can not be reflected by Eq. (2) that is derived based on the limit equilibrium condition. How to account for the drag velocity in theoretically evaluating the drag force is an interesting work, and further study is required.

3.4 Trajectory

The theoretical solution from Liu et al. (2013) is adopted to investigate the anchor trajectory together with the numerical analysis. Parameters necessary for the theoretical prediction can be found in Tables 1 and 6, in which b is the effective bearing width of the installation line that equals the diameter of the line, and ε is a parameter depending on the anchor line and soil properties, i.e., $\varepsilon = (s_{u0} + k\zeta)/k$ and ζ denotes the initial embedment depth of the horizontal line. The calculated values of ζ and ε are 0 and 3.33m, respectively. Trajectories obtained from numerical calculation and theoretical prediction for all anchor models are presented in Figure 11, which shows a better agreement between numerical and theoretical results except the rectangular anchor.

Figures 11 (e) and (f) show the trajectories from numerical and theoretical analysis, respectively. It is observed that the rectangular anchor has the highest drag embedment efficiency, i.e., the anchor has the largest penetration depth at the same drag distance. The reason is that the anchor trajectory is significantly influenced by the movement direction of the anchor θ_m and the drag angle at the shackle θ_a. The penetration depth increases with increasing values of θ_m and θ_a. Hence, the sum of θ_m and θ_a could be a key parameter to simply evaluate the drag embedment efficiency especially in numerical analysis. For example, the numerical sums are 35.9°, 25.0°, 28.6° and 27.9° for the rectangular anchor, Wedge 1, Wedge 2 and Wedge 3, respectively. For the three wedge anchors, Wedge 2 penetrates deeper than Wedge 1 and Wedge 3, because it has larger effective shear and bearing areas. Although the effective bearing area of Wedge 1 is larger than that of Wedge 3, the drag embedment efficiency of Wedge 1 is lower than that of Wedge 3 in the numerical analysis, which is contrary to the theoretical predictions. In theoretical analysis, the effective shear and bearing areas directly determine the penetration depths of the wedge anchors. The larger the areas are, the higher the drag embedment efficiency becomes.

During analyzing the anchor trajectory, the relationship between the drag distance and the horizontal displacement of the anchor needs to be clarified. Comparisons between the drag distance S and the horizontal displacement x_a at the end of drag distance from both numerical and theoretical results are listed in Table 7. It can be observed that the relative error of the horizontal displacement to the drag distance for the rectangular anchor is larger than that for the wedge anchor, because the penetration depth

Table 6 Parameters in the theoretical prediction from Liu et al. (2013)

Anchor	b (m)	s_u (kPa)	N_{cl}	N_{cf}	ε (m)	θ_m (°)	α
Rectangular	0.1	5+1.5z	10.8	9.7	3.33	0	0.42
Wedge 1						-12	0.46
Wedge 2							0.51
Wedge 3							0.47

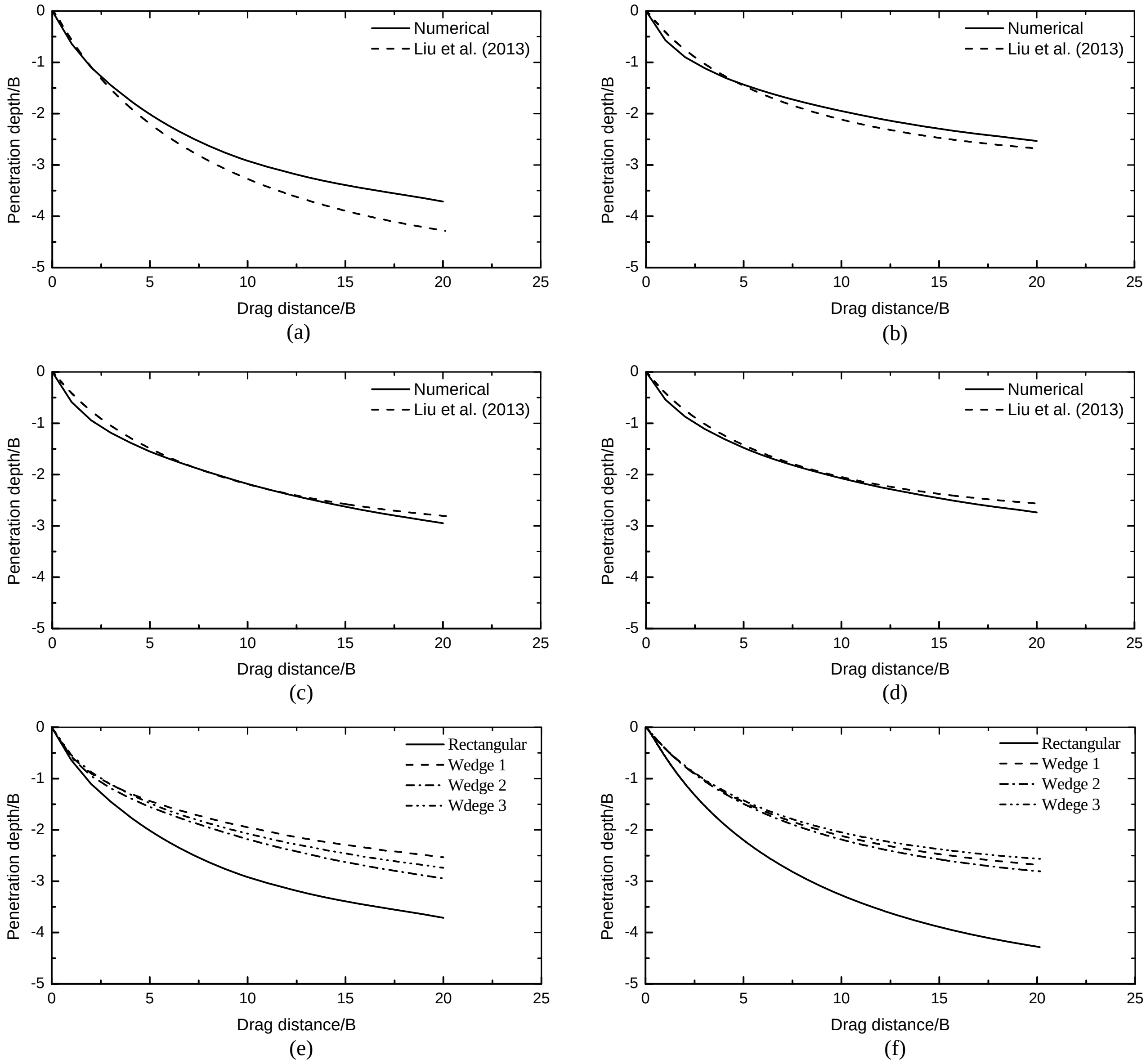

Figure 11 Trajectories from numerical and theoretical analysis: (a) rectangular anchor; (b) Wedge 1; (c) Wedge 2; (d) Wedge 3; (e) numerical; (f) theoretical

Table 7 Comparison between drag distance and horizontal displacement

Anchor	S (B)		x_a (B)		$(x_a - S)/S$ (%)	
	Numerical	Theoretical	Numerical	Theoretical	Numerical	Theoretical
Rectangular	20		20.63	20.81	3.15	4.05
Wedge 1	20		20.38	20.40	1.90	2.00
Wedge 2	20		20.43	20.43	2.15	2.15
Wedge 3	20		20.41	20.37	2.05	1.85

of the rectangular anchor is bigger than that of the wedge anchor and hence the horizontal displacement is larger. Table 7 proves that the difference between the drag distance and the horizontal displacement is very small for all anchor models. In the practical engineering, the anchor trajectory can not be observed. However, the drag distance can be well controlled by the movement of an AHV. It is clearly known from numerical and theoretical analysis that the horizontal displacement of the anchor nearly equals the drag distance.

3.5 Expression to estimate the ultimate embedment depth

The ultimate embedment depth (UED) of drag anchors is a key parameter to evaluate the anchor performance, which directly influences the trajectory of the anchor. As the anchor reaches the UED, the anchor fluke approximately approaches a horizontal orientation, i.e., the movement direction of the fluke is nearly horizontal (Liu et al. 2010a). This motion property was adopted generally in predicting the anchor trajectory in soils (Stewart 1992; Neubecker and Randolph 1996; Thorne 1998; O'Neill et al. 2003). Based on numerical simulation results, a method for estimating the UED of the anchor is proposed.

Although complex interaction happens between the anchor and ins tallation line during installation, two conditions of the anchor must be conformed, i.e., at the initial time, $z_a = 0$ and $\theta_{ah} = 0$; at the UED, $z_a = z_{UED}$ and $\theta_{ah} = \theta_a$. Note that z_a denotes the penetratio n depth of the fluke herein. Our earlier study (Zhang et al. 2014) p roposed a relationship between the penetration depth of the anchor and the drag angle to the horizontal at the shackle, which is expressed as to obtain a nearly complete trajectory or the UED by numerical simulations using the CEL technique is very time-consu ming. However, the UED of drag anchors can be estimated emplo ying Eq. (3) and limited numerical simulation results.

$$z_{UED} = \left(\frac{\theta_a}{\theta_{ah}}\right)^2 z_a \tag{3}$$

The curves from Eq. (3) utilizing the numerical results togethe r with the anchor penetration depth at the end of drag distance z_{end} are presented in Figure 12. It can be observed that the ultimat e embedment depths calculated by Eq. (3) (after the drag distance of 1B) are almost constant, which conforms with the physical reali ty, i.e., there is only one z_{UED} for a specific anchor during installat ion. The movement directions of the fluke to the horizontal at the end of drag distance are 3.8°, 2.3°, 3.6° and 3.4° for the rectangula r anchor, Wedge 1, Wedge 2 and Wedge 3, respectively, which me an the flukes are approaching the horizontal but do not completely reach the UED. Values of z_{end} are 3.70B, 2.53B, 2.95B and 2.74 B for the rectangular anchor, Wedge 1, Wedge 2 and Wedge 3, res pectively. The mean value of z_{UED}, denoted by $\overline{z_{UED}}$, is also calcu lated according to Eq. (3). Values of $\overline{z_{UED}}$ are 4.64B, 2.98B, 3.52 B and 3.28B for the rectangular anchor, Wedge 1, Wedge 2 and W edge 3, respectively. The difference between values of z_{end} and $\overline{z_{UED}}$ for all anchor models is reasonable. Therefore, Eq. (3) can b e simply used to estimate the UED of the anchor by employing nu merical simulation results.

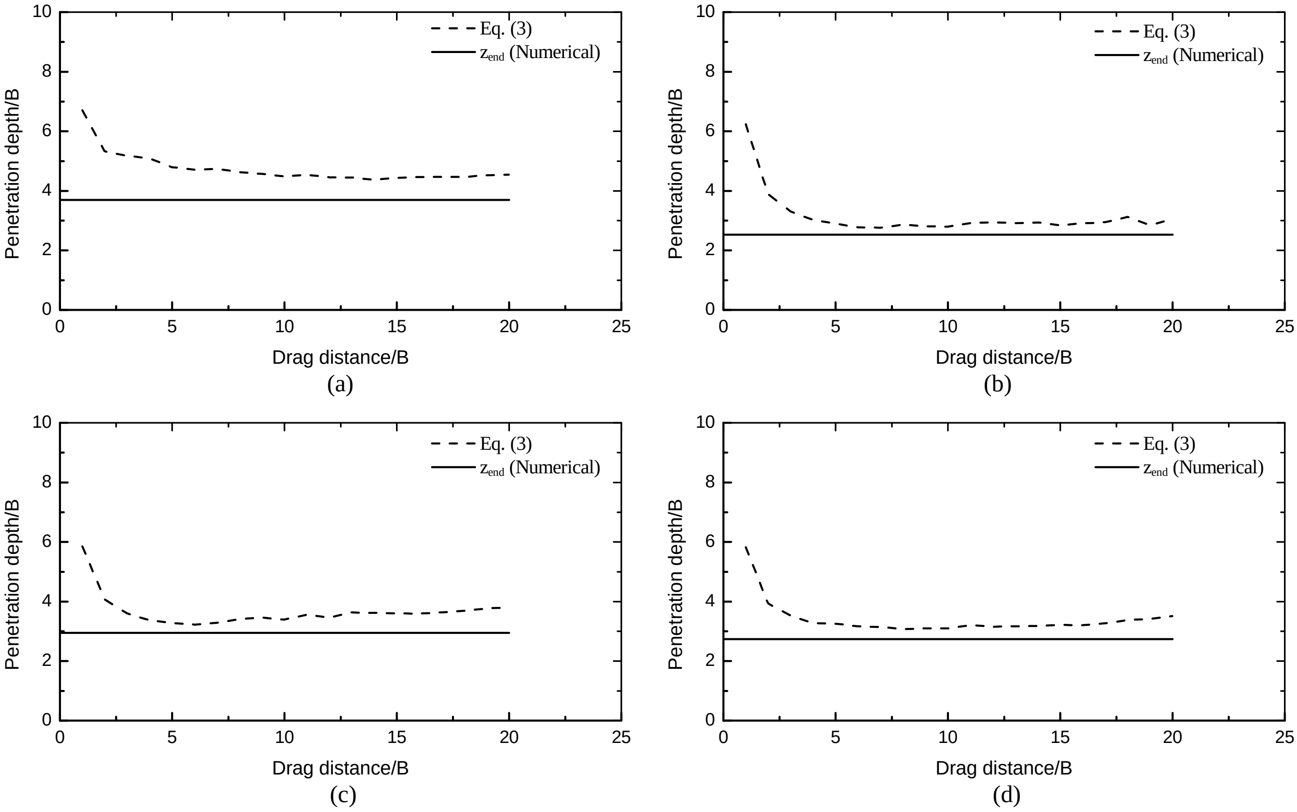

Figure 12 Comparison between Eq. (3) and z_{end}: (a) rectangular anchor; (b) Wedge 1; (c) Wedge 2; (d) Wedge 3

4. CONCLUSIONS

During installation of a drag anchor in seabed soils, the fundamental properties of the anchor such as the movement direction of the fluke, the drag angle and drag force at the shackle and the anchor trajectory in soils are closely relevant to the penetration mechanism and kinematic behavior of the drag anchor. In the present work, a large deformation finite element analysis using a coupled Eulerian-Lagrangian approach is performed to simulate the installation process of drag anchors with different fluke sections.

By investigating the dependency of the numerical simulation results on the mesh density and drag velocity, a method for determining the reasonable mesh density and drag velocity is proposed, which is established between the key dimensions of the anchor and the anchor line. It is observed that the drag velocity has a significant effect on the drag force. The drag force increases with increasing drag velocity. How to evaluate the relationship between the drag force and the drag velocity in the numerical simulation is a meaningful work and further study is required.

The numerical analysis proves that the movement directions at different points on the fluke are nearly the same and not influenced by the anchor geometry. Hence, the movement direction of the centre of mass of the fluke is reasonable to represent the movement direction of the anchor. However, the movement directions are very different for the rectangular and wedge models, as demonstrated from both the numerical and theoretical analysis. The numerical analysis reveals that the rectangular anchor moves along a plane lying 4.7° below its bottom fluke surface, and the wedge anchor travels along a plane lying between its top and bottom surfaces but approaching the bottom surface. The theoretical analysis reveals that the movement direction of either the rectangular or the wedge anchor is along the bottom surface of the fluke. The numerical analysis also proves that for the wedge anchors, the movement direction of the anchor increases a little with decreasing ratio of the top length to the bottom length.

It is confirmed by the numerical analysis that the drag angle at the shackle to the top surface of the fluke keeps almost a constant during installation. Based on the numerical and theoretical analysis, it is found that the drag angle is closely relevant to the anchor geometry. The drag angle will be determined by the specific shank angle and the connecting type between the shank and the fluke, although the numerical calculated drag angles are smaller than the theoretical predictions.

It is revealed from the numerical and theoretical analysis that the anchor geometry has a significant effect on the anchor trajectory, and the drag embedment efficiency of the rectangular anchor is higher than that of the wedge anchor. The anchor trajectory is significantly influenced by the movement direction of the anchor and the drag angle at the shackle. The sum of the movement direction and the drag angle could be a key parameter to simply evaluate the drag embedment efficiency especially in numerical analysis. The larger the sum is, the higher the drag embedment efficiency becomes. It is also examined that the horizontal displacement of the anchor in soils nearly equals the drag distance of the AHV. This is important for positioning drag anchors in practical engineering.

Finally, based on numerical simulation results, a method for estimating the UED of drag anchors is proposed, through which the UED can be simply estimated with limited numerical simulation results.

5. ACKNOWLEDGEMENTS

Financial support from the National Natural Science Foundation of China (Grant nos. 51179124 and 50979070) and Tianjin Research Program of Application Foundation and Advanced Technology (14JCZDJC39900) is greatly acknowledged.

6. REFERENCES

Aubeny, C.P., Murff, J.D., and Kim, B.M. (2008), "Prediction of anchor trajectory during drag embedment in soft clay", International Journal of Offshore Polar Engineering, 18, Issues 4, pp314-319.

Aubeny, C.P., and Chi, C. (2010), "Mechanics of drag embedment anchors in a soft seabed", Journal of Geotechnical and Geoenvironmental Engineering, 136, pp57-68.

Dahlberg, R., and Strom, P.J. (1999), "Unique onshore tests of deepwater drag-in plate anchors", Proceedings of the 31st Offshore Technology Conference, Houston, USA, May.

Dassault Systemes (2010), ABAQUS, version 6.10 documentation.

Degenkamp, G., and Dutta, A. (1989), "Soil resistances to embedded anchor chain in soft clay", Journal of Geotechnical Engineering, 115, Issues 10, pp1420-1438.

Det Norshke Veritas (DNV), (2000), "Design and installation of fluke anchors in clay", Recommended Practice RP-E301, DNV RP-E301.

Elkhatib, S., and Randolph, M.F. (2005), "The effect of interface friction on the performance of drag-in plate anchors", Frontiers in Offshore Geotechnics: ISFOG 2005, Gourvenec & Cassidy (eds), Taylor & Francis Group, London, UK.

Liu, H.X., Li, Y., Yang, H.T., Zhang, W., and Liu, C.L. (2010a), "Analytical study on the ultimate embedment depth of drag anchors", Ocean Engineering, 37, pp1292-1306.

Liu, H.X., Zhang, W., Zhang, X.W., and Liu, C.L. (2010b), "Experimental investigation on the penetration mechanism and kinematic behavior of drag anchors", Applied Ocean Research, 32, Issues 4, pp434-442.

Liu, H.X., Liu, C.L., Yang, H.T., Li, Y., Zhang, W., and Xiao, Z.J. (2012a), "A novel kinematic model for drag anchors in seabed soils", Ocean Engineering, 49, pp33-42.

Liu, H.X., Zhang, W., Liu, C.L., and Hu, C. (2012b), "Movement direction of drag anchors in seabed soils", Applied Ocean Research, 34, pp78-95.

Liu, H.X., Liu, C.L., Zhao, Y.B., and Wang, C. (2013), "Reverse catenary equation of the embedded installation line and application to the kinematic model for drag anchors", Applied Ocean Research, 43, pp80–87.

Merifield, R.S., Sloan, S.W., and Yu, H.S. (2001), "Stability of plate anchors in undrained clay", Geotechnique, 5, Issues 12, pp141-153.

Neubecker, S.R., and Randolph, M.F. (1996), "The performance of drag anchor and chain system in cohesive soil", Marine Georesources and Geotechnology, 14, pp77–96.

O'Neill, M.P., Randolph, M.F., and Neubecker, S.R. (1997), "A novel procedure for testing model drag anchors", Proceedings of the 7th International Offshore and Polar Engineering Conference, Honolulu, USA, May, pp939-945.

O'Neill, M.P., and Randolph, M.F. (2001), "Modelling drag anchors in a drum centrifuge", International Journal of Physical Modelling in Geotechnics, 2, pp29-41.

O'Neill, M.P., Bransby, M.F., and Randolph, M.F. (2003), "Drag anchor fluke-soil interaction in clays", Canadian Geotechnical Journal, 40, Issues 1, pp78-94.

Ruinen, R.M. (2004), "Penetration analysis of drag embedment anchors in soft clay", Proceedings of the 14th International Offshore and Polar Engineering Conference, Toulon, France, May, pp531-537.

Rowe, R.K. (1978), "Soil structure interaction analysis and its application to the prediction of anchor behavior", PhD Thesis, University of Sydney, Australia.

Stewart, W.P. (1992), "Drag embedment anchor performance prediction in soft soils", Proceedings of the 24th Offshore Technology Conference, Houston, USA, May, pp241-248.

Thorne, C.P. (1998), "Penetration and load capacity of marine drag anchors in soft clay", Journal of Geotechnical and Geoenvironmental Engineering, 124, pp945–953.

Vivatrat, V., Valent, P.J., and Ponterio, A.A. (1982), "The influence of chain friction on anchor pile design", Proceedings of the 14th Offshore Technology Conference, Houston, USA, May, pp153-156.

Yen, B.C., and Tofani, G.D. (1984), "Soil resistance to stud link chain", Proceedings of the 16th Offshore Technology Conference, Houston, USA, May, pp479-483.

Zhang, W., Liu, H.X., Zhao, Y.B., and Yue, Y.Z. (2014), "Interactional properties between drag anchor and installation line", Journal of Geotechnical and Geoenvironmental Engineering, 140, Issues 2, 04013018, pp1-11.

Zhao, Y.B., and Liu, H.X. (2013), "Large deformation finite element analysis of the anchor line embedded in seabed soils", Proceedings of the 32nd International Conference on Ocean, Offshore and Arctic Engineering, Nantes, France, June.

Zhao, Y.B., and Liu, H.X. (2014), "Numerical simulation of drag anchor installation by a large deformation finite element technique", Proceedings of the 33rd International Conference on Ocean, Offshore and Arctic Engineering, San Francisco, USA, June.